On Cr2N precipitation mechanisms in high nitrogen austenite

Patrícia Almeida Carvalho, Izabel Fernanda Machado, Guillermo Solorzano, Angelo Fernando Padilha

On Cr2N precipitation mechanisms in high nitrogen austenite

Journal:	*Philosophical Magazine & Philosophical Magazine Letters*
Manuscript ID:	TPHM-07-Nov-0316
Journal Selection:	Philosophical Magazine
Date Submitted by the Author:	04-Nov-2007
Complete List of Authors:	Carvalho, Patrícia; Instituto Superior Tecnico, Departamento de Engenharia de Materiais Machado, Izabel; EPUSP, Mechanical Systems Solorzano, Guillermo; PUC-RIO, Materials Science Padilha, Angelo; EPUSP, Mechanical Systems
Keywords:	nitrides, transmission electron microscopy
Keywords (user supplied):	austenitic steels, discontinuos precipitation, twin fronts

On Cr_2N precipitation mechanisms in high nitrogen austenite

P. A. CARVALHO*†, I. F. MACHADO‡, G. SOLÓRZANO§, A. F. PADILHA¶

†IST, Department of Materials Engineering, Av. Rovisco Pais, 1049-001 Lisboa, Portugal

‡EPUSP, Department of Mechatronics and Mechanical Systems Engineering, Av. Prof. Mello Moraes, 2231, 05508-900 São Paulo, S.P. Brazil

§PUC-RIO, Department of Materials Science and Metallurgy, R. Marquês de São Vicente, 225, 22453-900 Rio de Janeiro, R.J. Brazil

¶EPUSP, Department of Metallurgical and Materials Engineering, Av. Prof. Mello Moraes 2463, 05508-900, São Paulo, S.P. Brazil

Precipitation mechanisms in a high-nitrogen (0.87 wt.%) fully austenitic 25Cr-5Ni (wt.%) steel have been studied after ageing at 900°C and 960ºC. Ageing induced discontinuous precipitation of Cr_2N from grain boundaries, discontinuous precipitation at twin fronts, continuous precipitation throughout the matrix, continuous precipitation in association with ferrite plate formation and also grain boundary precipitation in the form of both discrete precipitates and films.

The observed morphologies at the onset of discontinuous precipitation from grain boundaries suggest a Tu and Turnbull initiation mechanism. The orientation relation between Cr_2N and γ in well-developed lamellae is not strictly $(111)\gamma//(0001)Cr_2N$ and $[1\bar{1}0]\gamma//[1\bar{1}00]Cr_2N$. The fact that the process shows some orientation tolerance, together with the lamellae irregular and curved interfaces, indicates that minimization of the system interfacial energy does not play a key role during growth. In this precipitation mechanism,

twinning inside growing γ lamellae is associated with abrupt local changes in the growth direction.

In the case of cooperative growth at incoherent twin fronts, the irregular habit surfaces of Cr_2N point to a Fournelle and Clark type of initiation mechanism. At early precipitation stages, the interlamellar spacing for cooperative growth at twin fronts is similar to the one observed for cooperative growth from grain boundaries (~100nm). It is proposed that the low growth efficiency observed at twin fronts results from lower diffusivity conditions at twin fronts as compared with grain boundaries.

Key words: Austenitic steels, nitrides, discontinuous precipitation, twin fronts, transmission electron microscopy.

1. Introduction

In a supersaturated alloy, volume or continuous precipitation (CP) tends to compete with cellular or discontinuous precipitation (DP). The question of which mechanism predominates depends on the mobility and density of discontinuous reactions fronts as well as on the incubation periods for each mechanism. As the temperature increases, bulk diffusion becomes faster favouring volume precipitation [1,2] and, as a result, close to the solvus temperature CP prevails [3]. Under precipitation regimes where DP dominates, any previous or concomitant volume precipitation reduces the amount of chemical driving energy available for both initiation and propagation of DP.

Discontinuous precipitation is a nucleation and growth solid-state transformation involving grain boundary migration into adjacent supersaturated grains. The transformation produces two-phase cells consisting of alternate lamellae (or rods) of a precipitated phase in a

solute depleted matrix. The accepted initiation mechanisms for DP are the 'pucker mechanism' of Tu and Turnbull [4,5] and the Fournelle and Clark mechanism [6]. Both treat DP initiation within the general framework of grain boundary migration. In the 'pucker mechanism' an embryo, developing at an angle with respect to a grain boundary (GB), causes the boundary to be locally deflected by the torque term associated with the interfacial tension balance at the triple point. If the interfacial energy conditions are favourable, the GB tends to migrate until the higher energy broad face is incorporated in the lower interfacial energy grain (figure 1 (a)). The process is iterated to form a group of parallel precipitates. Although this mechanism has been proven operative, it is critically dependent on the crystallographic orientation across the GB and on the habit planes of the precipitates, and is hence not universal. In the Fournelle and Clark mechanism, precipitation occurs on an already moving boundary. The GB is locally pinned but still allowed to continue migrating between the precipitates (figure 1 (b)). In contrast with the previous, this mechanism does not require any especial interfacial energy conditions, and is probably operating whenever no preferential matrix/precipitate habit plane can be observed which, is generally the case (for reviews see refs [7-9]).

The growth process associated with DP in alloys containing both interstitial and substitutional solutes is distinct from the pattern observed in binary substitutional systems. In these systems the material transport is caused exclusively by interfacial diffusion at the reaction front and therefore the composition of the untransformed matrix and the velocity of the reaction fronts remain constant [7-9]. On the other hand, in interstitial/substitutional systems the key factor governing the compositional redistribution is the difference between the partitioning processes of the two types of solutes. In these conditions although diffusion of the substitutional solute at the reaction front is the rate-controlling effect at the initial stages of

precipitation, long-range volume diffusion of the interstitial solute is the essential aspect at the later stages [10]: the fast long-range interstitial diffusion reduces the supersaturation of the untransformed matrix, decreasing the migration rate of the reaction front and widening the interlamellar spacing. This means that no steady-state is reached, in contrast with binary substitutional alloys.

Although Cr_2N precipitation can occur continuously in austenitic stainless steels, at high nitrogen supersaturations lamellar colonies ("false pearlite") formed by a DP reaction tend to predominate at temperatures around 900^{o}C [11-16]. Nevertheless, at later precipitation stages long-range volume diffusion of nitrogen induces retardation of new nucleation events and inhibition of active reaction fronts that eventually cease to migrate. This results in incomplete decomposition even though the matrix may still be supersaturated in nitrogen and the reaction driving force is not equal to zero [10,13,15,16].

Discontinuous precipitation in multi-component systems involving both substitutional and interstitial solutes, such as high nitrogen austenitic stainless steels, is still not fully investigated. In particular, little attention has been given to initiation and growth mechanisms in nitride precipitation. Furthermore, competition between Cr_2N precipitation mechanisms and its association with other phase transformations require further analysis. The purpose of this work is to study the decomposition of a nitrogen austenite, aiming at a more extensive understanding of precipitation mechanisms.

2. Materials and methods

Nitrogen has been added to a standard type duplex stainless steel DIN W.-Nr.1.4460 by pressurized electroslag remelting [13]. The resulting steel was received in the form of a

forged bar with the following composition (wt.%): 25.1Cr; 1.9Mo; 5.5Ni; 1.5Si; 1.20Mn; 0.03C and 0.87N. Chromium nitride precipitation occurs in the current steel up to 1050^{o}C [11], therefore the solution annealing treatment had to be carried out at higher temperatures. On the other hand, the stability domain of ferrite starts at temperatures as low as 1300 ºC, and annealing at higher temperatures results in duplex microstructures [11]. Annealing at 1250 ºC presented the best compromise to achieve complete dissolution of nitrides and to simultaneously guarantee the absence of ferrite. The as-received material was solution annealed at 1250^{o}C for 1 hour and subsequently water quenched. Solution annealed samples were aged at 900 ^{o}C for 90 s and at 960^{o}C for 2 h, followed by water quenching.

Crystal structures and lattice parameters of the predominant phases have been determined by X-ray diffraction (XRD) using CuKα1. The average grain size of the annealed austenite was determined using the linear intercept method in optical micrographs. The lattice parameters of the annealed and aged (960^{o}C for 2 h) austenite were determined with the least-squares method using (222), (400), (331) and (420) reflections. The amount of ferromagnetic phases was measured by magnetic induction using a Fischer Magnetoscope®M11D with a 0.1% vol. ferrite detection limit.

Preliminary observation of the microstructures was performed by scanning electron microscopy (SEM) with a Hitachi S2400 instrument after standard metallographic preparation. TEM samples have been prepared by grinding 3 mm discs down to 100-150 μm of thickness, followed by either (i) electropolishing in 100 ml perchloric acid (60%), 200 ml glycerine and 700 ml methanol at -30 ^{o}C with 0.3 to 0.4A for a few seconds; or by (ii) double-side dimpling down to 20 μm of thickness and ion-milling with argon to electron transparency. TEM observations were carried out using a PHILIPS microscope at 120 kV, a JEOL 200C microscope at 200 kV and a Hitachi H-8100 instrument operated at 200 kV, which was

equipped for Energy Dispersive Spectroscopy (EDS) with a Si(Li) detector protected by a polymeric window. Microdiffraction experiments and EDS analyses were performed with a 15 nm probe diameter.

2. Results and discussion

Magnetic induction measurements, XRD and SEM observations showed the absence of ferrite in the solution annealed material [11]. The annealed austenite presented an average grain size of 65 μm and a 0.3622_5 nm lattice parameter. The TTT diagram previously obtained using metallographic observations, X-ray diffraction and magnetic induction [11] enabled to expect the presence of Cr_2N in the austenitic matrix for the short ageing treatment (90 s at 900°C), whereas both Cr_2N and ferrite should be present after the longer ageing treatment (2 h at 960 °C) [11].

2.1 Discontinuous vs continuous Cr_2N precipitation

Electron microscope observations revealed that ageing for 2 h induced the competition of discontinuous vs continuous precipitation mechanisms. DP resulted in an extensive presence of lamellar colonies, with well-defined reaction fronts characteristic of cooperative growth. A continuous process could also be inferred from the presence of discrete precipitates. However, although some austenite grains evidenced only volume precipitation, the predominance of the lamellar morphology confirmed higher transformation efficiency for the DP reaction. Figure 2 exhibits a typical microstructure, where both DP and CP regions can be observed. The arrow indicates precipitation at a grain boundary. The grain labelled as A decomposed continuously, exhibiting precipitates with lenticular or faceted morphologies.

Globular/rod-like precipitates can be observed in grain B, which also presents discontinuous fronts.

Figure 3 presents bright-field TEM images showing the onset of DP at early ageing stages. In figure 3 (a) the nitride lamellae are developing at an angle with respect to the GB, which caused the boundary to be locally deflected and resulted in a morphology closely resembling the configuration proposed by Tu and Turnbull [4,5] (see figure 1 (a)). GB migration at a definite angle with the habit planes is also clearly evident in figure 3 (b). The interlamellar spacing at early precipitation stages is around 100 nm.

Figure 4 shows a colony with alternating lamellae of Cr_2N and solute depleted austenite growing from the supersaturated austenite after ageing for 2h at 960°C. In spite of the apparent intragranular condition, a homogeneous nucleation should not be inferred as the aggregate is probably a cross-section of a larger colony nucleated heterogeneously at a GB somewhere else. Although the nucleation behaviour of the colony cannot be discussed, its crystallographic features allow a deeper understanding of the γ/Cr_2N cooperative growth. The selected area diffraction (SAD) pattern presented in figure 4 shows that the OR between the two lamellar phases is close to the relation described in the literature [10,17]: $(111)\gamma//(0001)Cr_2N$ and $[1\bar{1}0]\gamma//[1\bar{1}00]Cr_2N$. However, there is a slight misorientation (15 mrad) as the solid lines in the diffraction pattern indicate. The reaction fronts are roughly perpendicular to the compact $(111)_\gamma$ and $(0001)_{Cr_2N}$ planes, however, local changes in growth direction affected the Cr_2N/γ lamellar interfaces which do not correspond to specific habit planes. The orientation tolerance, together with the lamellae irregular and curved interfaces, indicates that the transformation is unable to take full advantage of potentially low interfacial energy configurations during the growth process. Consequently, minimization of the system interfacial energy is not critical for the lamellar configuration adopted during growth, which

may result from an initially favoured nucleation of Cr_2N on $(111)_\gamma$ planes and from kinetic reasons related to comparable growth rates of the compact planes for both phases.

A similar precipitation behaviour has been described for the Ni-Sn system [18].

The lattice parameter (a) determined for austenite after 2 h at 960 ^oC by XRD is 0.3616_4 nm [11]. The following experimental relation for this austenite a = 0.00272 wt.% N + 0.36002 nm [19], enables to estimate a nitrogen content of 0.6 wt.%. This shows that after two hours of ageing treatment there is still a high nitrogen supersaturation in the austenitic matrix, in agreement with the growth pattern expected for interstitial/substitutional systems.

Twin domains inside austenite lamellae were frequently observed in well developed DP colonies. Twinning was associated with abrupt modifications in the growth direction of the Cr_2N lamellae, as illustrated in figure 5 (arrows). The ledges and the twin front morphology in the magnified inset of figure 5 indicate that the original crystallographic orientation of the lamella outgrew the mirrored one after another growth inflection. These results show that the shape changes associated to the presence of twin domains are able to accommodate shear strain during the solid state transformation. Stacking fault termination/initiation under similar circumstances has been observed in discontinuous precipitation of Ni_3Sn [18]. The irregular morphology of the nitride lamellae in figure 5 indicates again that minimization of the total interfacial energy of the system is not a key factor for the lamellar configuration adopted during growth.

Figure 6 (a) shows typical isolated intragranular Cr_2N precipitates, exhibiting lenticular and faceted morphologies and displaying complex interfacial contrast. The lenticular precipitate presents a low-index OR with the matrix. Contrarily to the 0001 spot in the $[1\bar{1}00]$ microdiffraction pattern, the 0001 spot in the $[11\bar{2}0]$ microdiffraction pattern cannot be generated by dynamical scattering effects and confirms a trigonal structure as opposed to a

hcp-based one [20]. The strong dislocation contrast observed around these precipitates points to partial coherence between the phases, at least at early precipitation stages.

Figure 6 (b) shows a region where globular/rod-like precipitates have been observed. The fringe contrast surrounding the particles results from a combined effect of thickness changes related to the shape of the precipitates and extinction at the inclined interfaces. Diffraction experiments enabled to identify these precipitates as Cr_2N. No preferred OR with the matrix could be found and dislocation contrast was not observed around these globular precipitates. Similar globular/rod-like Cr_2N precipitates have been previously reported in high nitrogen Cr-Mn austenitic steel [21].

A close inspection at figure 2 reveals that precipitate morphologies analogous to the ones displayed in figure 6 (a) can be found in region A, whereas the ones of figure 6 (b) correspond to a region similar to B. The precipitation mechanism of lenticular and faceted precipitates is clearly continuous; however globular/rod-like Cr_2N may result from an irregular cooperative process occurring at terminal ageing stages.

Figure 7 shows ferrite plates growing in a region where nitrides have precipitated continuously. Ferrite growth involves heavy nitrogen segregation that contributes to the formation of nitride precipitates at the δ/γ interfaces. These precipitates were able to grow across ferrite plates and into the matrix. The orientation relation between ferrite and austenite is of the Kurdjomov-Sachs type. EDS analyses and diffraction experiments carried out with these precipitates enabled to identify the Cr_2N phase. The ferrite volume fraction determined by magnetoscope measurements in the material aged at 960^{o}C for 2 h is ~5 %.

2.2 Cr_2N precipitation at incoherent twin fronts

Figure 8 shows an isolated twin plate growing in austenite. Chromium-rich precipitates lie along the twin front (see EDS spectrum). As it would be unlikely for the twin front to meet on its way a row of aligned precipitates, one can assume these have precipitated at the interface. This means that either precipitation has blocked the twin plate growth or this is an example of grain boundary migration and the two phases would subsequently grow cooperatively forming a discontinuous precipitation aggregate. This type of behaviour has been reported for $M_{23}C_6$ [22]. However, to the authors' best knowledge, it has not been described for chromium nitride precipitation. A SAD pattern of the set is shown in figure 8 (c). This diffraction pattern is similar to the one presented in figure 5, where the phases present the same orientation relation: $(111)\gamma//(111)\gamma_T//(0001)Cr_2N$ and $[1\bar{1}0]\gamma//[1\bar{1}0]\gamma_T//[1\bar{1}00]Cr_2N$. The extra satellites and streaking observed in figure 8 (c) result, respectively, from double diffraction effects and from the precipitate alignment along the twin front. A microdiffraction pattern of a precipitate under the same orientation is shown in (d).

The set was studied under another crystallographic orientation, where a complex diffraction configuration was observed as shown in figure 9 (a). Careful diffraction experiments and pattern simulation for the 3 crystals (which were associated considering the above OR and jointly rotated) enabled to interpret this diffraction pattern as follows: (i) the main reflections match the diffraction pattern of the matrix, as shown in figure 9 (b)); (ii) there is a perfect overlap between reflections corresponding to the mirror related austenite domains, as can be inferred by comparing figures 9 (b) and (c)); (iii) the magnified inset in figure 9 (a)) shows spots around the austenite reflections originating from Cr_2N, that under this orientation exhibits a pattern configuration similar to the twin domain one, as can be seen in figure 9 (d)); (iv) Cr_2N reflections are multiplied by double diffraction effects.

Figure 10 shows another twin plate growing into the austenite matrix and displaying nitride precipitation at its front. In this case, cooperative growth between the two phases is evident. Contrarily to the similar cooperative growth observed at twin fronts for $M_{23}C_6$ [22], Cr_2N lamellae do not present well-defined habit planes. In view of the irregular morphologies and curved habit surfaces of the precipitates in Figs. 8 and 10, a mechanism of the Fournelle and Clark type is likely to be operative: the Cr_2N precipitates appear in an already migrating boundary, growing thereafter cooperatively with the solute depleted twin domain with no preferential matrix/precipitate habit plane.

The interlamellar spacing at twin fronts was similar to the one observed at the early precipitation stages of DP initiated at grain boundaries, i.e., ~100 nm (compare figures 3 and 10). However, cooperative growth at twin fronts was incipient when compared with DP from grain boundaries and the question arises as to why growth at twin front conditions is less efficient.

Although the twin front is not fully coherent (dislocations are generally associated with this type of glissile interface), it can be expected to exhibit less distortion in the individual atomic positions when compared with an incoherent grain boundary. This causes increased activation energy for substitutional diffusion and therefore decreased diffusion permeability [23,24]. As a result, the incipient growth of CrN + γ_T aggregates may be justified by lower Cr diffusivity conditions at the twin front as compared with grain boundaries. It is worth mentioning that, contrarily to DP from grain boundaries, the precipitates protrude significantly at the reaction front (compare figures 8 and 10 with figure 3), indicating that the interface between the parent and twinned austenite, γ/γ_T, has lower mobility than the Cr_2N/γ interface. Alternatively, strain-fields at the twin front may also contribute to hinder growth: the high

coherency of the whole configuration is expected to limit the strain that a twin front can accommodate both in directions perpendicular and parallel to the coherent mirror planes.

2.3 Grain boundary precipitation

Discrete Cr_2N precipitates were frequently observed at grain boundaries. Figure 11 shows precipitates displaying the usual preferred OR with the matrix; some of these precipitates grew from the grain boundary into the upper region (see A). The crystallographic orientation of austenite is the same at both sides of the GB original position, in agreement with a GB migration process: the bottom grain swept the above region, growing cooperatively with *some* of the Cr_2N particles precipitated at the GB. This type of configuration is frequent at the initiation sites of DP colonies. The curved morphology of the precipitate lamellae reflects the low influence of interfacial energy on the cooperative growth process.

Figure 12 shows another example of precipitation at a GB. In this case, there is an approximately continuous film of nitride at the GB and the austenite phase has a different crystallographic orientation on each side. The diffraction pattern corresponds to a mirror orientation relation, indicating that the Cr_2N film separates twinned regions and that precipitation occurred at the mirror plane. The orientation relation between the phases is $(111)\gamma//(111)\gamma_T//(0001)Cr_2N$ and $[1\bar{1}0]\gamma//[1\bar{1}0]\gamma_T//[1\bar{1}00]Cr_2N$ (compare the diffraction patterns in figure 12 and figure 9 (a)). Interfacial considerations seem to justify the fact that under this crystallographic configuration the precipitates were able to grow into a film.

5. Conclusions

Precipitate morphologies at the onset of Cr_2N discontinuous precipitation from grain boundaries point to a Tu and Turnbull initiation mechanism. The OR between γ and Cr_2N lamellae in DP colonies is not strictly: $(111)\gamma//(0001)Cr_2N$ and $[1\bar{1}0]\gamma//[1\bar{1}00]Cr_2N$. Furthermore, local changes in growth direction affect the lamellar interfaces which do not correspond to specific habit planes. This indicates that the transformation is unable to take full advantage of potentially lower interfacial energy configurations during the growth process. Consequently, minimization of the system interfacial energy during growth is not crucial for the lamellar configuration adopted, which seems to result from an initially favoured nucleation of Cr_2N on $(111)_\gamma$ planes together with comparable growth rates along the compact planes for both phases. Twinning inside austenite lamellae in well developed DP colonies was related to growth inflections and indicates that the shape changes associated with the twin domains are able to accommodate shear strain developed during the solid state transformation.

Precipitate morphologies at the onset of Cr_2N discontinuous precipitation from twin fronts point to a Fournelle and Clark initiation mechanism. Cr_2N precipitates at twin fronts presented a $(111)\gamma//(111)\gamma_T//(0001)Cr_2N$ and $[1\bar{1}0]\gamma//[1\bar{1}0]\gamma_T//[1\bar{1}00]Cr_2N$ orientation relation with the mirror related austenite domains. Cooperative growth at twin fronts was incipient when compared with the one observed for DP colonies. The sluggish growth of CrN + γ_T aggregates can be justified by lower Cr diffusivity conditions at the twin front. Strain-fields at the twin front may also contribute to hinder growth in this discontinuous precipitation mechanism.

Austenite grains with no signs of discontinuous reaction fronts exhibited continuously precipitated Cr_2N. Discrete precipitation was also observed in association with ferrite plate formation and at grain boundaries. Nevertheless, a higher efficiency for DP from grain

boundaries was evident. The present results indicate that interfacial considerations do not play a critical role in the higher precipitation efficiency of this mechanism.

6. References

[1] M. Hillert, Metall Trans **3** 2729 (1972)

[2] M. Hillert, Acta Metall **30** 1689 (1982)

[3] D. Duly, J. P. Simon, Y. Brechet, acta Metall Mater **43** 101 (1995)

[4] K.N. Tu and D. Turnbull, Acta Metall. **369** 1317 (1967).

[5] K.N. Tu, Metall. Trans. **3** 2769 (1972).

[6] R.A. Fournelle and J. B. Clark, Metall. Trans. **3** 2757 (1972).

[7] W. Gust, Phase transformations (The Institution of metallurgists, London, 1979), Vol 1, pp.II 27-68.

[8]D.B. Williams and Butler, Int. Mater. Rev. **26** 153 (1981).

[9]D.Y. Yoon, Int. Mater. Rev. **40** 149 (1995).

[10] M. Kikuchi, M. Kajihara and S.K. Choi, Mater. Sci. Eng. **A146** 131 (1991).

[11] I.F. Machado and A.F. Padilha, Steel Res. **67** 285 (1996).

[12] W.E. Voice and R.G. Faulkner, J. Mater. Sci. **22** 4221 (1987).

[13] P. Pant, P. Dahlmann, W. Schlump and G. Stein, Steel Res. **58** 18 (1987).

[14] R.G. Faulkner, Mater. Sci. Tech. **9** 118 (1993).

[15] F. Vanderschaeve, R. Taillard and J. Foct, J. Mater. Sci. **30** 6035 (1995).

[16] N.C. Santhi Srinivas and V.V. Katumbarao, Scripta Mater. **37** 285 (1997).

[17] A.J. Ramirez, J.C. Lippold and S.D. Brandi, Met. Mater. Trans. **A34** 1575 (2003).

[18] P.A. Carvalho, M. Sijbolts, B.J. Kooi and J.Th.M De Hosson., Acta Mater. 48 4203 (2000).

[19] I.F. Machado, PhD thesis: Escola Politécnica da Universidade de São Paulo, Brazil, (1996).

[20] T.H. Lee, C.S. Oh, H.N. Han, C.G. Lee, S.J. Kim and S. Takaki, Acta Cryst. **B61** 137 (2005).

[21] E. Ruedl and G. Valdré, J. Mater. Sci. **23** 3698 (1988).

[22] T. Sourmail and H.K.D.H. Bhadeshia, Metall. Mater. Trans. **A36** 23 (2005).

[23]A.P. Sutton and R.W. Balluffi, Interfaces in Crystalline Materials, Elsevier Sceince, Oxford, 1995.

[24] I. Kaur, Y. Mishin, and W. Gust, Fundamentals of Grain and Interphase Boundary Diffusion, Honh Wiley, Chichester, 1995.

Figure 1 – Successive stages in DP initiation according to the (a) Tu and Turnbull [1,2] and (b) Fournelle and Clark [3] mechanisms.

Figure 2 – Typical microstructure of the material aged at 960°C for 2 hours evidencing both DP and CP. Grain A exhibits lenticular and faceted precipitates resulting from a continuous process. Globular precipitates can be observed in region B. The arrow points to precipitates at a grain boundary.

Figure 3 – Onset of chromium nitride discontinuous precipitation at grain boundaries at an early ageing stage (90 s at 900°C).

Figure 4 – (a) DP colony in an austenite grain (aged at 960°C for 2 h). (b) Diffraction pattern of the colony exhibiting 15 mrad of misorientation between the lamellar phases.

Figure 5 – Twin domains (γ_T) within austenite (γ) lamellae in a well developed DP colony (aged at 960°C for 2 h). Reciprocal lattice cells of the twin variants are indicated in the diffraction pattern. The mirror plane presents steps of tens of nanometres (magnified inset).

Figure 6 – (a) Lenticular and faceted Cr_2N precipitates in austenite (aged at 960°C for 2 h) and respective SAD and microdiffraction patterns (the lenticular precipitate presents a low-index OR with the matrix). (b) Globular/rod-like Cr_2N precipitates and microdiffraction pattern obtained from one precipitate (aged at 960°C for 2 h).

Figure 7 – Cr_2N growing across ferrite plates (a) and (b) together with microdiffraction patterns and EDS spectrum obtained at the numbered regions: (1) and (2) correspond to δ-ferrite, (3) and (4) to Cr_2N (aged at 960°C for 2 h).

Figure 8 – (a) A twin plate in austenite aged at 960°C for 2 h. (b) Magnified detail showing Cr nitride at the twin front. (c) SAD of the whole set corresponding to the $(111)\gamma//(111)\gamma_T//(0001)Cr_2N$ and $[1\bar{1}0]\gamma//[1\bar{1}0]\gamma_T//[1\bar{1}00]Cr_2N$ orientation relation (the diffraction pattern is rotated in relation to the image, the slight streaking is parallel to the twin front trace in (a) and (b)). (d) Microdiffraction pattern of the lower precipitate under the same orientation as (c)).

Figure 9 - (a) SAD corresponding to the whole twin front set shown in figure 8 under another crystallographic orientation. (b) SAD pattern obtained at the surrounding matrix under the same orientation as (a). The circled spots in (b) match exactly the ones of the twin domain pattern presented in (c). (d) Microdiffraction pattern of the lower precipitate under the same orientation as (a). The orientation relation between the phases is $(111)\gamma//(111)\gamma_T//(0001)Cr_2N$ and $[1\bar{1}0]\gamma//[1\bar{1}0]\gamma_T//[1\bar{1}00]Cr_2N$.

Figure 10 – Twin front exhibiting cooperative growth with Cr_2N precipitates (aged at 960°C for 2 h).

Figure 11 – Grain boundary precipitation (aged at 960°C for 2 h). The SAD pattern matches Cr_2N, which exhibits the usual preferred OR with austenite. Both γ regions have the same crystallographic orientation indicating that the observed lamellar Cr_2N precipitation is the result of a GB migration process.

Figure 12 – (a) Continuous nitride film precipitated at a twin boundary (aged at 960°C for 2 h) under tilt condition 1, where the contrast difference between the adjacent austenite grains demonstrates different crystallographic orientations. (b) Magnified detail of the selected region in (a) under tilt condition 2, where the two austenite regions display similar contrast. (c) SAD pattern of the set under tilt condition 2 (for interpretation refer to figure 9).

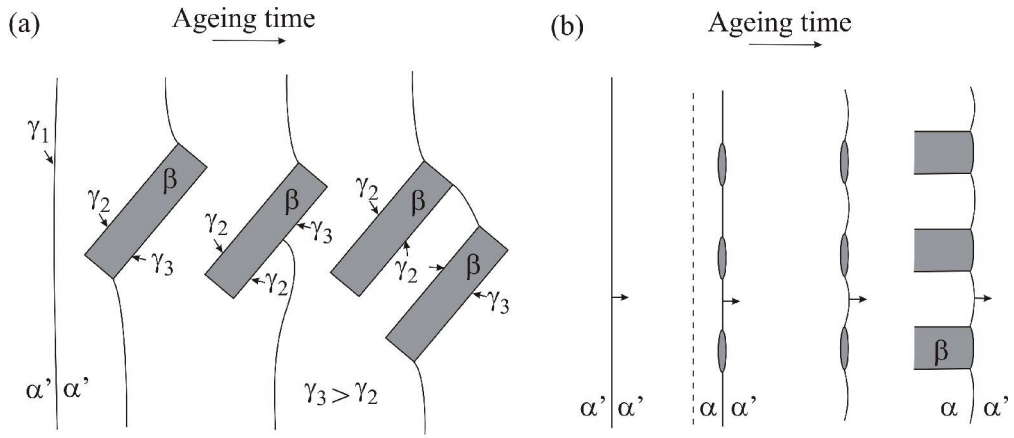

Figure 1
292x131mm (300 x 300 DPI)

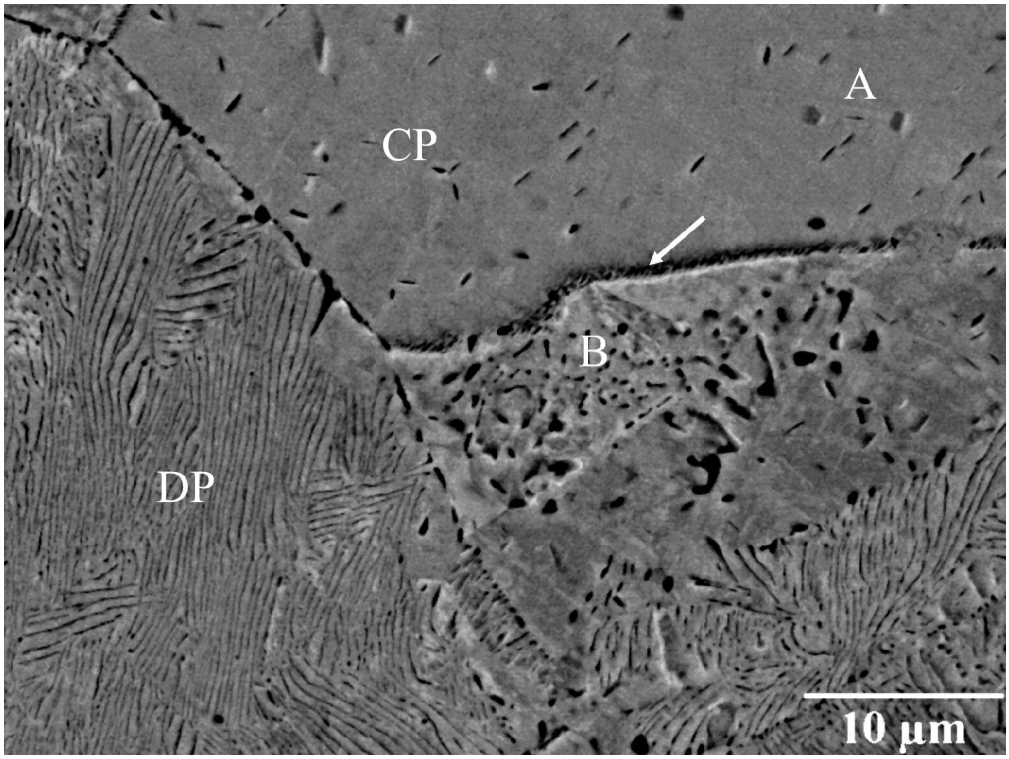

Figure 2
137x102mm (300 x 300 DPI)

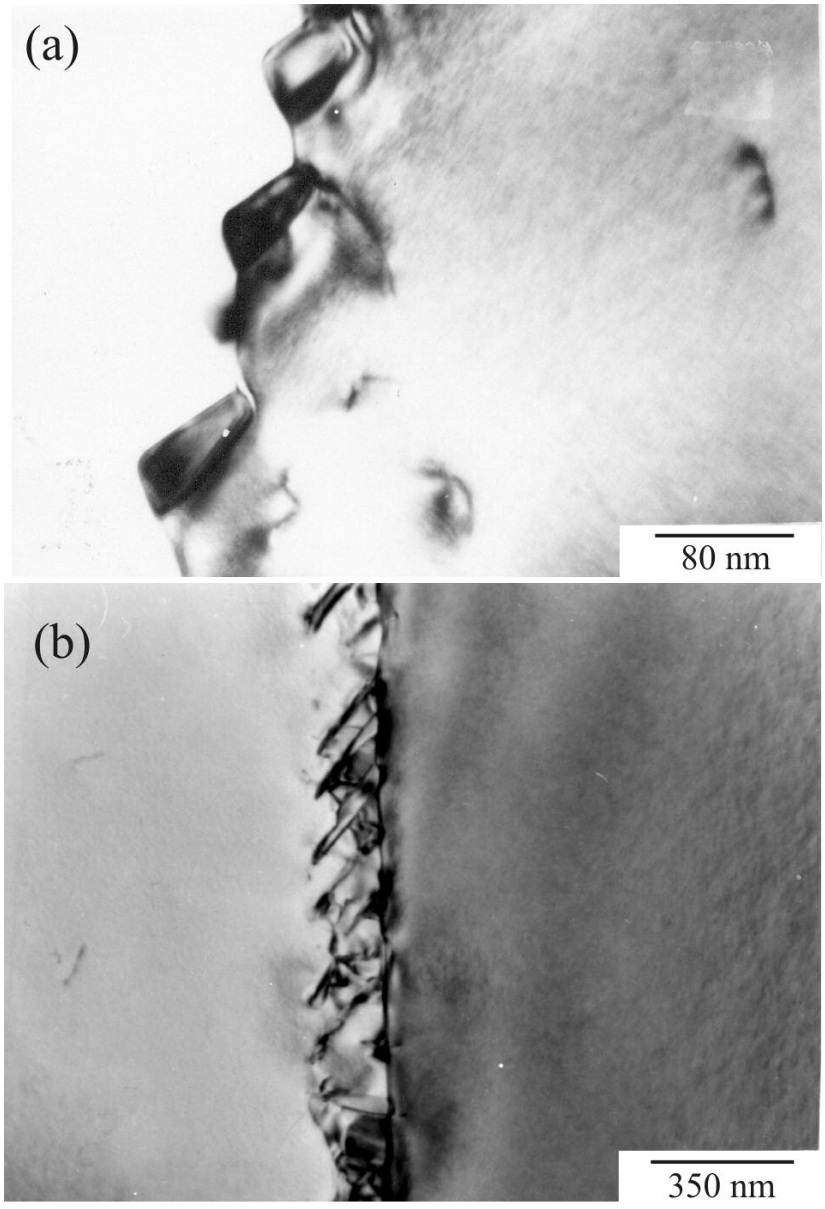

Figure 3
80x118mm (300 x 300 DPI)

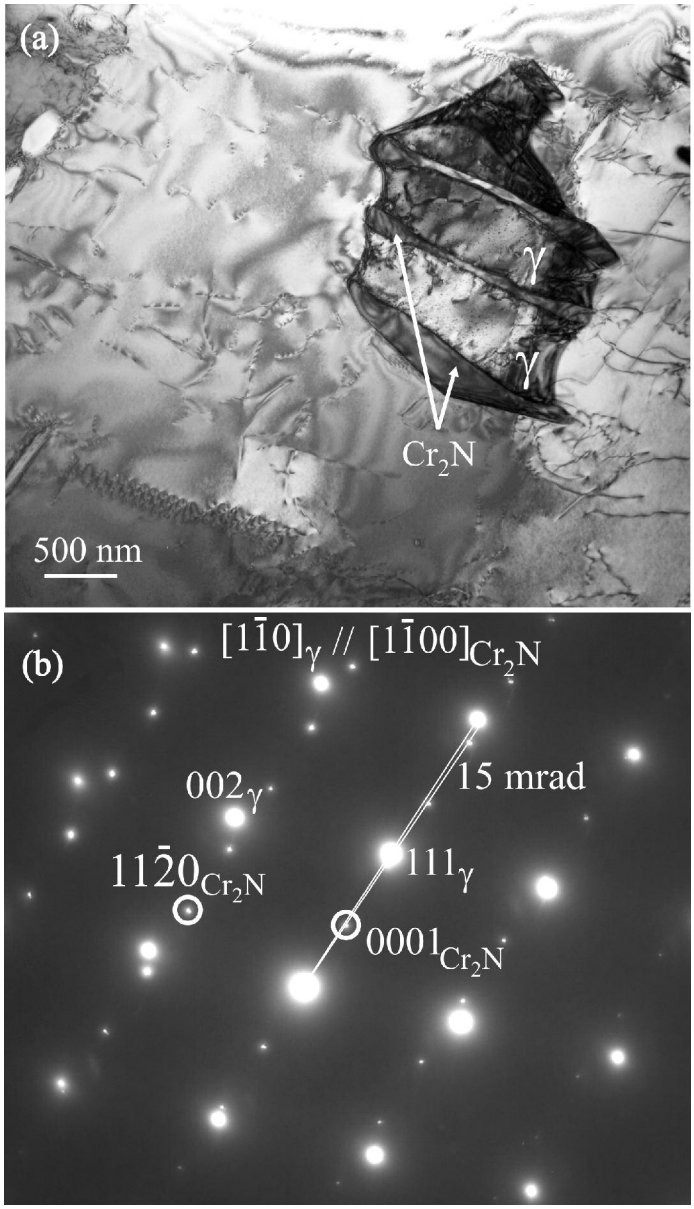

Figure 4
120x210mm (300 x 300 DPI)

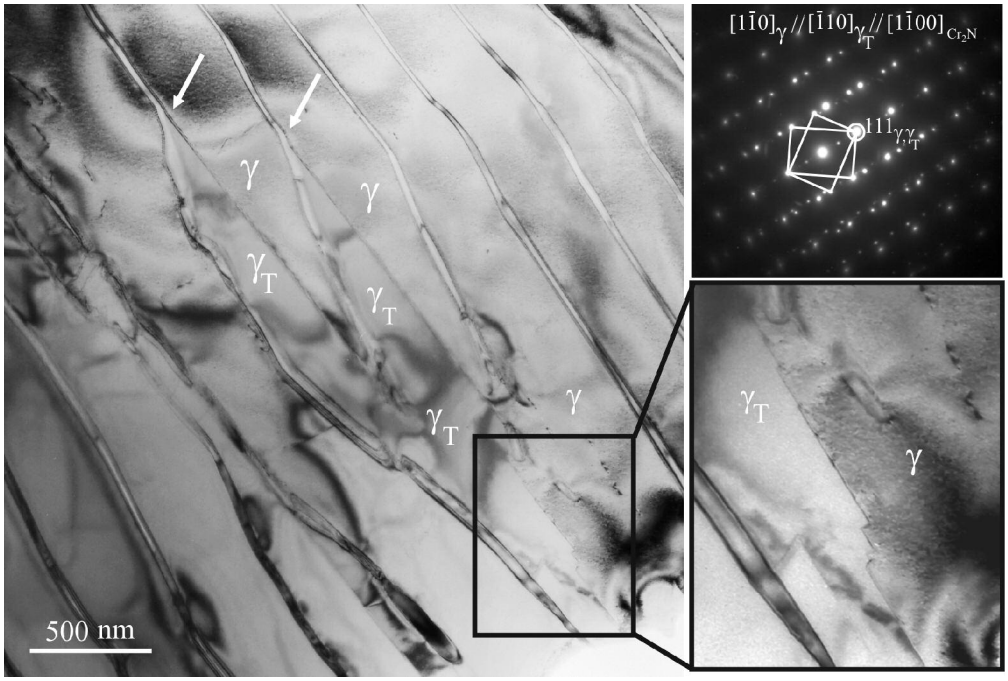

Figure 5
144x97mm (300 x 300 DPI)

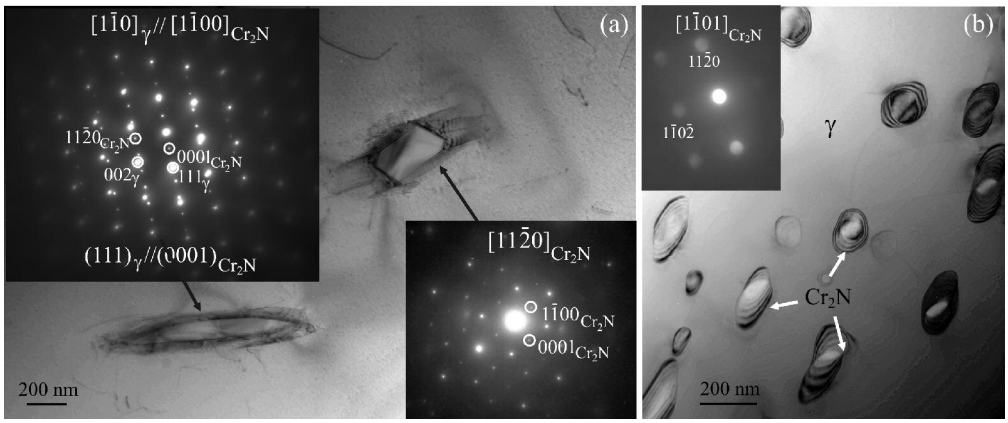

Figure 6
214x89mm (300 x 300 DPI)

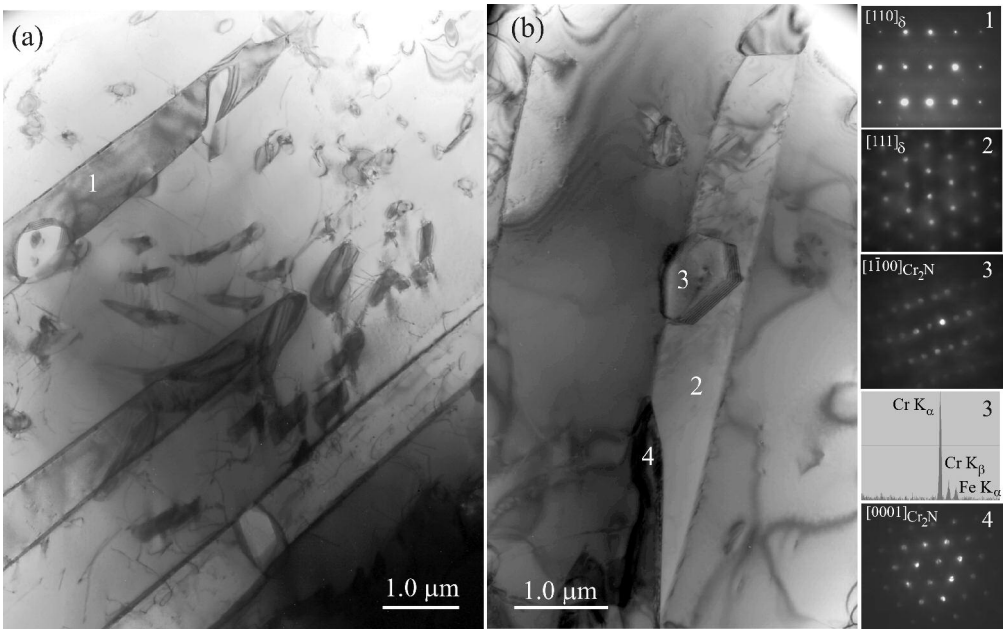

Figure 7
271x170mm (300 x 300 DPI)

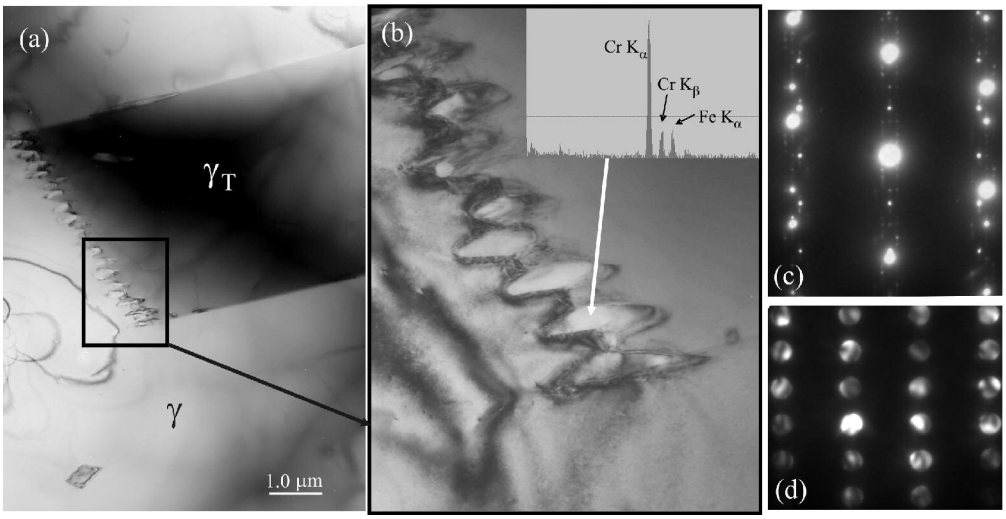

Figure 8
189x97mm (300 x 300 DPI)

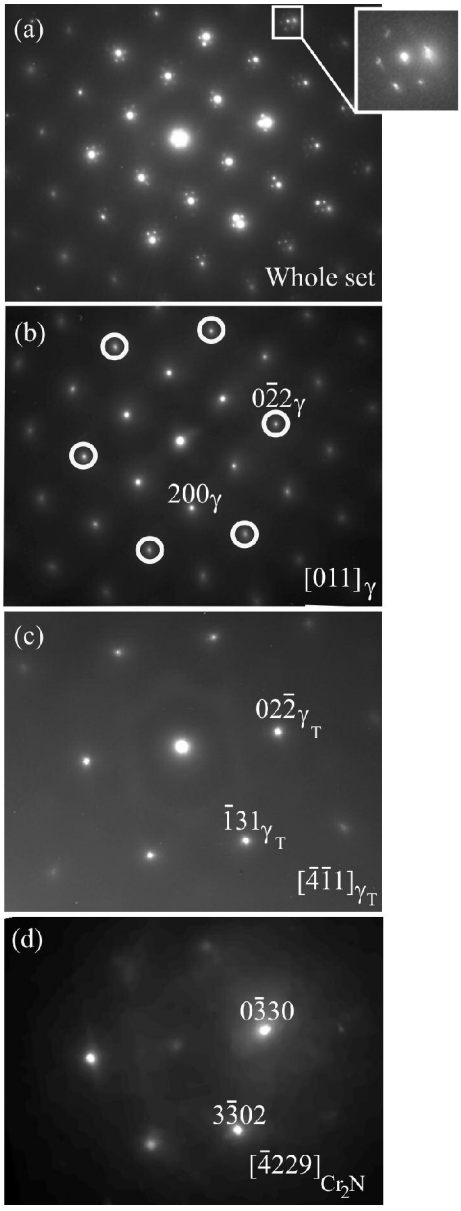

Figure 9
70x184mm (300 x 300 DPI)

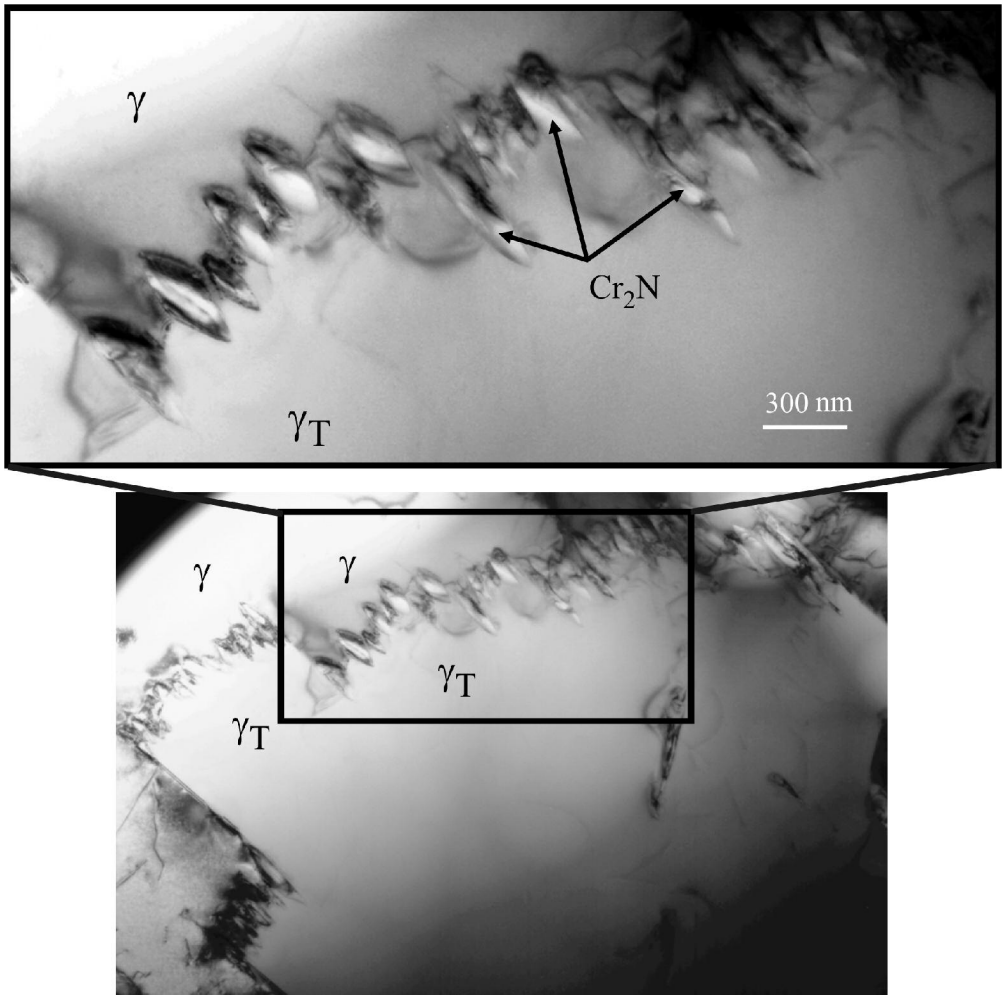

Figure 10
167x166mm (300 x 300 DPI)

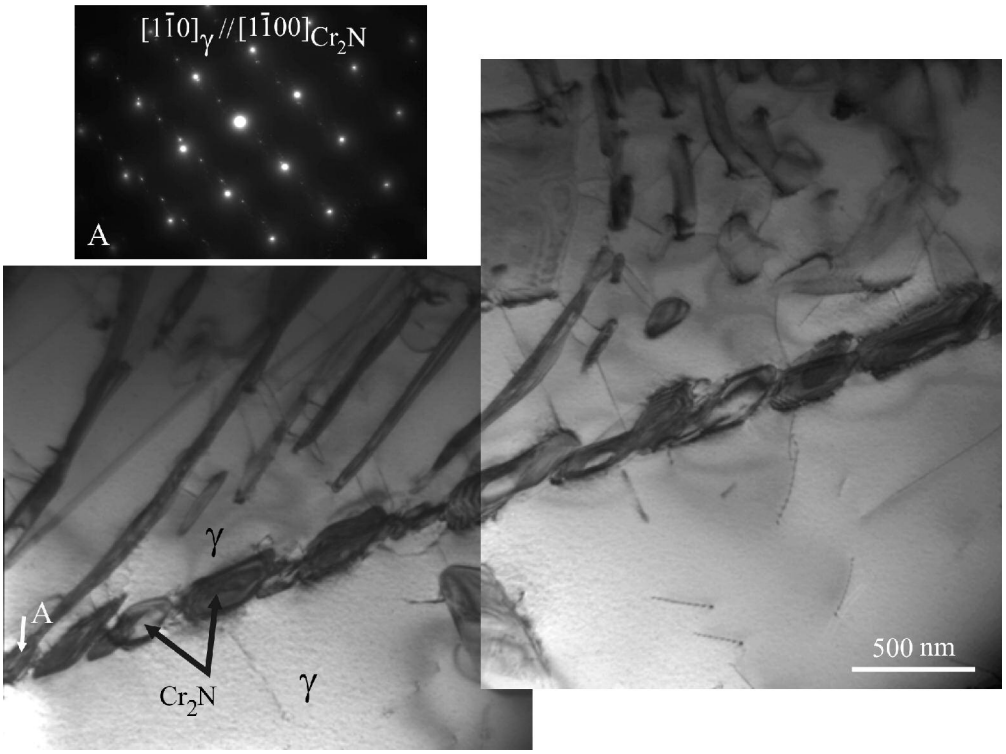

Figure 11
178x140mm (300 x 300 DPI)

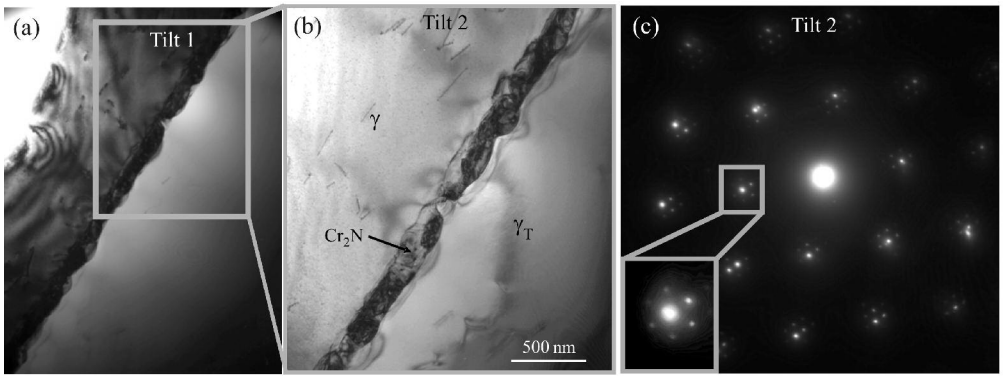

Figure 12
230x86mm (300 x 300 DPI)